Molecular Therapy
Nucleic Acids
Original Article

Modulation of miR-29 influences myocardial compliance likely through coordinated regulation of calcium handling and extracellular matrix

Xiaoming Zhang,[1] Jared M. McLendon,[1] Bailey D. Peck,[1] Biyi Chen,[1] Long-Sheng Song,[1] and Ryan L. Boudreau[1]

[1]Department of Internal Medicine, Fraternal Order of Eagles Diabetes Research Center, Abboud Cardiovascular Research Center, Carver College of Medicine, University of Iowa, Iowa City, IA, USA

MicroRNAs (miRNAs) control the expression of diverse subsets of target mRNAs, and studies have found miRNA dysregulation in failing hearts. Expression of miR-29 is abundant in heart, increases with aging, and is altered in cardiomyopathies. Prior studies demonstrate that miR-29 reduction via genetic knockout or pharmacologic blockade can blunt cardiac hypertrophy and fibrosis in mice. Surprisingly, this depended on specifically blunting miR-29 actions in cardiomyocytes versus fibroblasts. To begin developing more translationally relevant vectors, we generated a novel transgene-encoded miR-29 inhibitor (TuD-29) that can be incorporated into a viral-mediated gene therapy for cardioprotection. Here, we corroborate that miR-29 expression and activity is higher in cardiomyocytes versus fibroblasts and demonstrate that TuD-29 effectively blunts hypertrophic responses in cultured cardiomyocytes and mouse hearts. Furthermore, we found that adeno-associated virus (AAV)–mediated miR-29 overexpression in mouse hearts induces early diastolic dysfunction, whereas AAV:TuD-29 treatment improves cardiac output by increasing end-diastolic and stroke volumes. The integration of RNA sequencing and miRNA-target interactomes reveals that miR-29 regulates genes involved in calcium handling, cell stress and hypertrophy, metabolism, ion transport, and extracellular matrix remodeling. These investigations support a likely versatile role for miR-29 in influencing myocardial compliance and relaxation, potentially providing a unique therapeutic avenue to improve diastolic function in heart failure patients.

INTRODUCTION

Heart failure (HF) is a leading cause of death, affecting ~2% of the world population.[1,2] Despite clinical advances, mortality rates remain high, with ~50% of patients dying within 4 years of disease onset; hence, studies to advance our insight into disease pathogenesis, risk factors for HF, and potential therapeutic targets remain essential. HF is a cardiomyopathy resulting from structural and functional deficits that impair the ability of the heart to output adequate blood supply to support the metabolic demands of the body. HF classifications primarily include HF with reduced ejection fraction (HFrEF; EF $\leq$40%) and HF with preserved EF (HFpEF; EF $\geq$ 50%). Although HFrEF is typically caused by ischemic or dilated cardiomyopathies, resulting in decreased contractility (i.e., impaired systolic function), HFpEF is associated with various risk factors and comorbidities, including hypertension, obesity/diabetes, and aging. These promote adverse myocardial remodeling (e.g., fibrosis, concentric myocyte hypertrophy), leading to ventricular stiffness and impaired relaxation and filling during diastole, thus decreasing stroke volume (SV) and cardiac output (CO). Given the increased incidence of these risk factors around the world, the incidence of HFpEF is rising and expected to soon surpass HFrEF. [2]

Mechanistic studies have unveiled several important biological pathways in HF pathogenesis, including perturbations in cardiomyocyte sarcomere structure/function, calcium handling, metabolism, electrophysiologic activity, and cell viability, as well as activation of proinflammatory and profibrotic signaling cascades, ultimately leading to myocardial demise.[3,4] These diverse disease processes coincide with significant alterations in myocardial gene expression patterns influenced by transcriptional and posttranscriptional regulatory controls, with many shared changes observed in hearts from human HF patients (e.g., explants) and animal models of HF.[5,6] Several groups have examined the potential roles for altered microRNA (miRNA) expressions and/or activities in HF,[7–9] since miRNAs serve as master regulators of the transcriptome and play critical roles in cardiac biology.[10] Mammalian genomes encode for ~2,000 unique miRNAs, which can incorporate into Argonaute (Ago)-RNA-induced silencing complexes (RISCs) to guide targeted mRNA destabilization through miRNA-mRNA base pairing, typically via the seed region (positions 2–8 of the miRNA) or other noncanonical base pairing modes.[11,12] These small RNAs are capable of regulating a diverse set of target mRNAs to uniquely coordinate a biological response, and their potential to serve as therapeutic targets is being investigated for a broad range of diseases.[13,14]

For example, expressions of miR-29 family members (miR-29a/b/c) are abundant in heart, altered in various cardiomyopathies, elevated

Received 20 June 2023; accepted 14 November 2023;
https://doi.org/10.1016/j.omtn.2023.102081.

Correspondence: Ryan L. Boudreau, Department of Internal Medicine, University of Iowa, 4334 PBDB, Iowa City, IA 52242, USA.
E-mail: ryan-boudreau@uiowa.edu

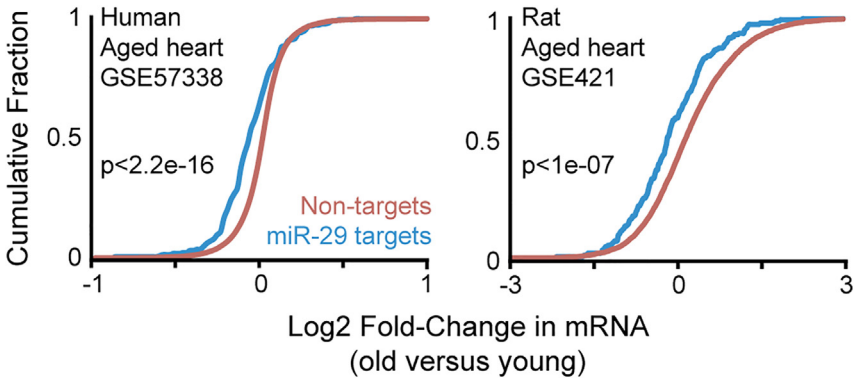

Figure 1. miR-29 target mRNAs are broadly reduced in aging human and mouse hearts

Publicly available transcriptome-wide gene expression data from studies, including cardiac tissue samples collected form young and old humans or mice, were analyzed to assess levels of miR-29 target mRNAs (blue, genes harboring empirically determined binding sites by Ago2 HITS-CLIP [high-throughput sequencing of crosslinked immunoprecipitates; Ago2-bound mRNA fragments][25]), relative to all other genes (red). For each dataset, cumulative fraction curves for miR-29 targets show clear leftward shifts, indicative of broad downregulation in aging hearts (for humans, ages 18–34 years versus 62–80 years, n = 21/group, and for rats, ages 4 months versus 22 months, n ≥ 5/group). GEO accessions (GSE no.) and Kolmogorov-Smirnov test p values are shown.

in diabetic/obese subjects, and increased in aging.[15–20] The miR-29 family is highly conserved across species, including humans and rodents, and is predicted to engage many of the same target sites within shared genes across vertebrates; for example, of 1,012 miR-29a/b/c target genes predicted in mice, 952 are also predicted targets in humans (per the TargetScan database[11]). Many of these shared targets are involved in extracellular matrix (ECM) remodeling, and much of the published work on miR-29 biology has focused on its antifibrotic functions with therapeutic implications.[15,21,22] However, recent studies have demonstrated that miR-29 reduction via cardiomyocyte-targeted genetic knockout or systemic pharmacologic blockade with anti-miRNA (anti-miR) oligonucleotides is sufficient to prevent stress-induced cardiac hypertrophy and fibrosis in mice.[23] Given that cell-targeted gene knockout is not readily translatable toward therapies and that chronic whole-body delivery of miR-29 anti-miRNAs would be expensive and likely to elicit other adverse peripheral consequences, there remains a need to begin generating more translational viral-based gene therapy vectors to inhibit miR-29 and assess their potential to improve heart function. Furthermore, although miR-29 is an established key player in cardiac biology and disease, the breadth of mRNAs that are functionally regulated (beyond prediction) by miR-29 in the heart have not been interrogated with adequate transcriptomic investigations. Here, we corroborate that myocardial miR-29 is more abundantly expressed and active in cardiomyocytes relative to fibroblasts and demonstrate that a transgene-encoded miR-29 inhibitor (Tough Decoy[24] [TuD-29]) is capable of blunting hypertrophic responses in cultured cardiomyocytes and mouse hearts subjected to pressure overload. In addition, we found that adeno-associated virus (AAV)–mediated miR-29 overexpression in mouse hearts induces signs of diastolic dysfunction and reduced CO, whereas AAV:TuD-29 treatment improves CO by increasing end-diastolic volume (EDV) and SV. Integration of RNA sequencing (RNA-seq) with miR-target interactome data reveals that miR-29 regulates genes involved in several key pathways relevant to HF—for example, calcium handling, lipid and ketone metabolism, cell stress, and ECM remodeling. Altogether, our findings highlight a potential role for miR-29 in regulating myocardial compliance and relaxation, supporting the notion that miR-29 may serve as an attractive therapeutic target to be considered further for the treatment of diastolic dysfunction and/or HFpEF.

RESULTS

miR-29 target genes are broadly downregulated in aged rodent and human heart tissues

Advanced age is a key recognized risk factor provoking HFpEF onset and progression. Several published reports indicate that miR-29 family member expressions in myocardial tissues increase with age[18,19]; however, there have been no published efforts to correlate these changes with broad decreases in miR-29 target genes in aged hearts. To address this, we reanalyzed publicly available data from previous studies that profiled transcriptomic alterations in hearts collected from humans and rodents of various ages. Cumulative fraction analyses were performed to compare fold change distributions of miR-29 targets, specifically those that we previously empirically identified in our biochemically determined human cardiac miR-mRNA target interactome dataset (obtained via Ago2 HITS-CLIP, high-throughput sequencing of crosslinked immunopreciptates).[25] Notably, in both humans and rats, we found that miR-29 target mRNAs overall are significantly shifted toward lower expression in aged heart tissues (for humans, ages 18–34 years versus 62–80 years, n = 21/group, GEO: GSE57338, and for rats, ages 4 months versus 22 months, n ≥ 5 each, GEO: GSE421; Figure 1).

miR-29 family members exhibit enriched expression in cardiac myocytes and provoke hypertrophy

Initial studies on miR-29 in the heart focused on miR-29 family member expressions in cardiac fibroblasts and antifibrotic roles through the suppression of several collagen genes.[15,26] However, our previous miRNA-target interactome studies in human heart tissues revealed that miR-29 engages several cardiomyocyte-enriched mRNA transcripts (e.g., those encoding Serca2a, Ryr2, and S100a1),[25] and more recent reports indicate that miR-29 expression levels are higher in cardiac myocytes, relative to fibroblasts.[23] We previously obtained similar findings when quantifying miRNA expressions in cardiomyocytes versus nonmyocytes (i.e., predominantly fibroblasts and endothelial cells) isolated from mouse hearts. The integrity of our cell

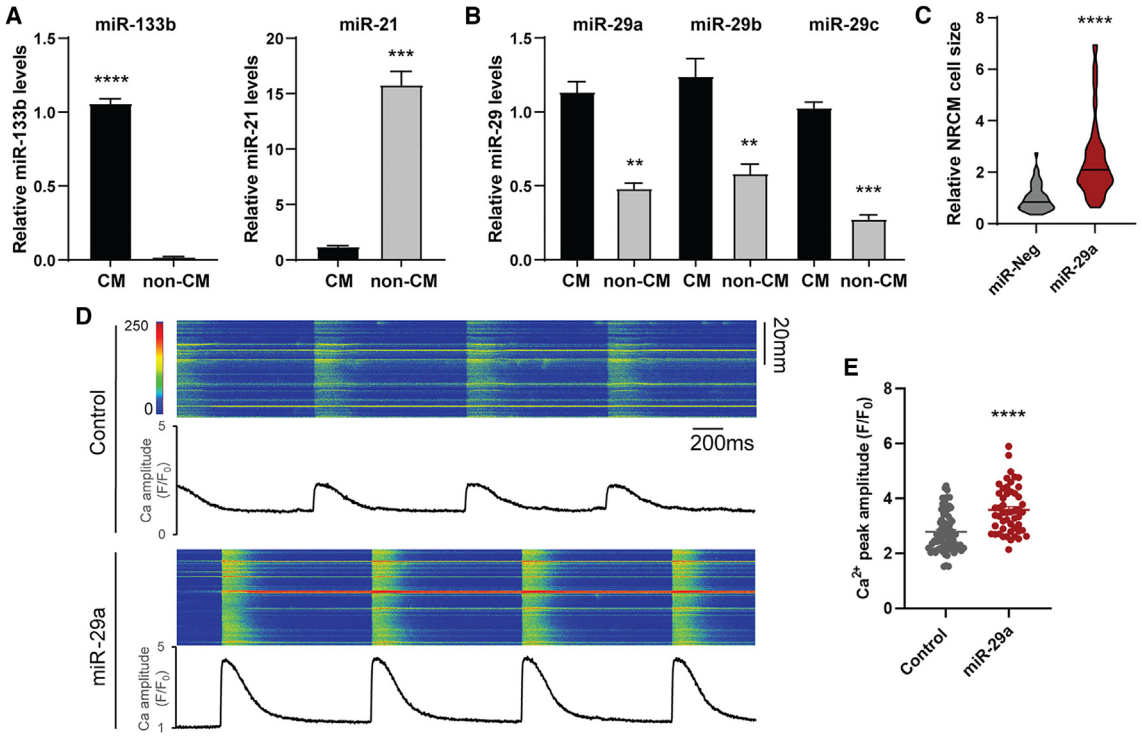

Figure 2. miR-29 expression is enriched in cardiomyocytes and promotes hypertrophy in NRCMs

Cardiomyocytes (CM) and non-CM cardiac cells (predominantly fibroblasts and endothelial cells) were harvested from adult mouse hearts (n = 3), and qPCR was performed to first quantify miRNA expressions for miR-133b (a known CM-enriched miRNA) and miR-21 (a known fibroblast-enriched miRNA) to assess integrity of the cell isolations (A). qPCR was then performed to quantify the expression levels of miR-29 family members a/b/c in the cell fractions (B). (A and B) Data were normalized to total RNA and plotted as mean ± SEM relative to the CM group. (C) NRCM cultures were cotransfected with GFP-expression plasmid and either miR-Neg or pre-miR-29a, and cell size of GFP^+ transfected NRCMs was assessed 72 h later and plotted as a violin plot ($n \geq 50$/group). (D and E) NRCMs were transfected with GFP-expression plasmid with or without miR-Neg (Control) or with pre-miR-29a, and live-cell confocal imaging of GFP^+ was done to assess steady-state Ca^{2+} transients with 30-s pacing at 1-Hz field stimulation. (D) Representative line scan images and traces are shown. (E) Quantitative data for Ca^{2+} transient peak amplitudes are plotted ($n > 50$/group). p values were determined by 2-tailed unpaired t tests. $^{**}p < 0.01$; $^{***}p < 0.001$; $^{****}p < 0.0001$.

isolations was verified by quantifying miR-133b and miR-21 levels, which are almost exclusively expressed in myocytes and fibroblasts respectively (Figure 2A). Quantification of miR-29 family members indicated that miR-29a/b/c each exhibit ∼2- to 4-fold higher expression in cardiomyocytes, relative to nonmyocytes (Figure 2A), corroborating the findings by Sassi et al.[23] This was further supported by a reanalysis of our human cardiac miRNA-target interactome data, which showed that biochemically isolated miR-29 targets favored cardiomyocyte versus fibroblast-enriched mRNAs by a factor of 2- to 4-fold, based both on the number of target sites identified and bulk miR-29 binding signal (i.e., summed peak heights) within genes that exhibit cell-enriched expression (defined as those with >5-fold differential mRNA expression in cardiomyocytes versus fibroblasts, based on available RNA-seq data from myocardial cell isolates, GEO: GSE58453) (Figure S1).[27]

In addition to calcium targeting genes, our previous miRNA-target interactome data also hinted at a role for miR-29 in cardiomyocyte hypertrophy (e.g., through targeting of PIK3R1 and GSK3B).[25] To test this, we transfected neonatal rat cardiomyocytes (NRCMs) with synthetic pre-miR-29a and observed a >2-fold increase in NRCM cell size at 48 h posttreatment, relative to scrambled miRNA negative control (miR-Neg) (Figure 2B). In parallel, we evaluated beat-by-beat calcium transients in NRCMs using live-cell confocal imaging. We found that miR-29a transfected NRCMs displayed substantially higher calcium transient peak amplitudes compared with controls (GFP and miR-Neg, $p < 0.001$), whereas T_{peak} (time to peak) and T_{50} (time to 50% from peak) were not significantly different between two groups (Figure 2C). These data are consistent with prohypertrophic and positive ionotropic effects mediated by miR-29, further corroborating and complementing findings from Sassi et al.,[23] who previously observed prohypertrophic effects induced by miR-29 in cardiomyocytes and mouse hearts.

Generation and functional validation of transgenic miR-29 inhibition vectors

Given that miR-29 inhibition through both genetic manipulation (i.e., knockout) and pharmacologic blockade (anti-miRs) conferred protection against cardiac hypertrophy in mice subjected to cardiac pressure overload,[23] we sought to develop a transgenic-encoded miR-29

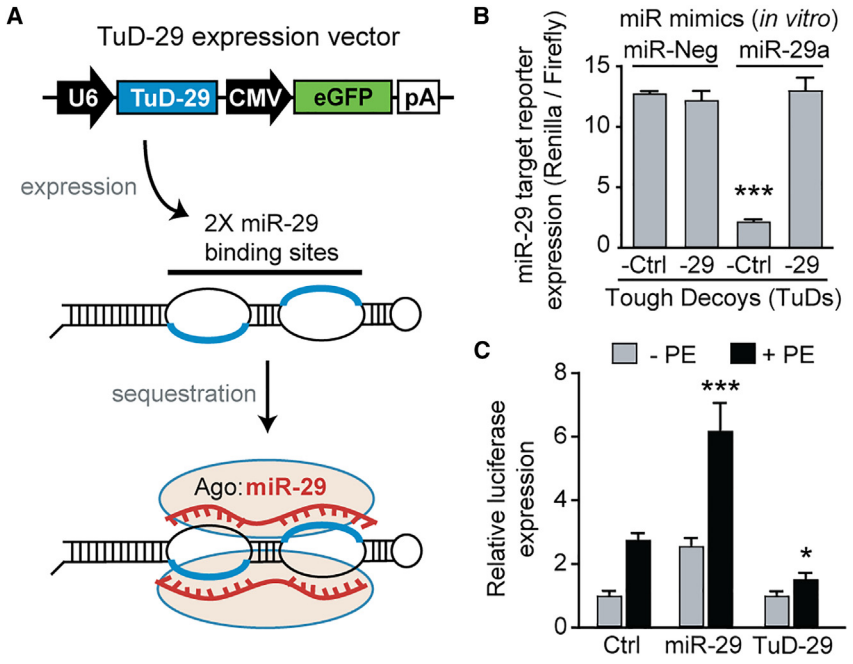

Figure 3. Overview and validation of miR-29 inhibitor expression construct

(A) Schematic of a custom plasmid expressing a Tough Decoy miR-29 inhibitor (TuD-29) under control of the U6 promoter and a cytomegalovirus (CMV)-driven GFP reporter. TuD-29 contains 2 high-affinity miR-29 binding sites capable of sequestering miR-29 family members and impeding their natural functions. (B) *In vitro* testing of the TuD-29 vector was done by cotransfecting N2a cells with a luciferase-based miR-29 target reporter plasmid (contains miR-29 seed binding sites in the 3′ UTR of R luciferase and coexpresses FF luciferase for normalization), synthetic miRNAs (miR-29a or scrambled negative control, miR-Neg), and plasmids expressing either TuD-29 or a scrambled control, TuD-Ctrl. Luciferase activities were measured at 48 h posttransfection and plotted as R/FF ratios (n = 4/group), indicating that TuD-29 almost completely blocks the ability of synthetic miR-29a to suppress the miR-29 target reporter. (C) NRCM cultures were co-transfected with luciferase expression plasmids and either TuD-Ctrl, miR-29a, or TuD-29 vectors and subsequently treated with PE (+PE) or not (−PE) to induce protein synthesis (a hallmark hypertrophic response). Luciferase activities were determined at 48 h posttreatment and plotted. Bar graphs represent mean ± SEM. p values were obtained using 1-way ANOVA with Sidak's test for multiple comparisons, miR-29a + TuD-Ctrl versus other groups (A) and miR-29a + PE or TuD-29 + PE versus TuD-Ctrl + PE (B). *$p < 0.05$; ***$p < 0.001$.

inhibitor for potential gene therapy application. For this, we generated a U6-driven TuD RNA that forms a highly stable stem-loop structure capable of sequestering two miR-29 molecules via high-affinity antisense binding sites (Figure 3A).[24] In initial cell transfection studies, the TuD-29 plasmid construct completely blunted the silencing of a miR-29 target luciferase reporter construct, relative to a scrambled control (TuD-Ctrl) in the presence of elevated miR-29 levels achieved via cotransfection of synthetic miR-29a mimic oligonucleotides (Figure 3B). We next tested whether our TuD-29 vector could block hypertrophic responses in NRCMs. For this, we used a straightforward assay to assess phenylephrine (PE)-induced increases in NRCM protein production, inferred from the synthesis and activity of two luciferase transgene reporters (Firefly [FF] and Renilla [R]) bicistronically encoded on a cotransfected plasmid. In control NRCMs, PE treatment induced a near 3-fold increase in luciferase activities, and miR-29 treatment alone led to a similar increase at baseline (i.e., no PE), which was further exacerbated following the addition of PE, providing added evidence supporting the prohypertrophic effects of miR-29 (Figure 3C). Most notably, miR-29 inhibition via TuD-29 plasmid cotransfection robustly blunted the PE-induced increases in reporter activities. Together, these data demonstrate the effectiveness of our custom TuD-29 expression vector in inhibiting miR-29 function and eliciting antihypertrophic effects in cultured cardiomyocytes.

TuD-29 transgenic mice resist pressure overload–induced cardiac hypertrophy and maintain calcium handling gene expressions

Genetic reduction of miR-29 family expression in multiallele knockout mice was previously shown to confer antihypertrophic effects in the setting of cardiac pressure overload, which was surgically induced by transverse aortic constriction (TAC).[23] To first test the effectiveness of our TuD-29 vector *in vivo*, we generated transgenic TuD-29-expressing mice (TuD-29-tg, backcrossed to C57BL/6J mice), which were viable with no overt phenotype, and subjected them to TAC surgeries, performed on ∼8-week-old TuD-29-tg and wild-type (WT) littermate control mice. At ∼10 weeks post-TAC, echocardiographic measures indicated that, as expected, WT mice showed clear signs of cardiac hypertrophy (increased heart size and mass, $p < 0.05$; Figure 4A; Table S1) and some mild dysfunction (trend toward decreased EF, which is typical of C57BL mice on the 6J background,[28,29]; Figure 4B) by echocardiography, relative to normal ranges established from echocardiographic data collected on >30 sham-surgery control C57BL/6J mice of similar age. Notably, TuD-29-tg mice showed a blunted response to TAC, relative to WT littermates, with significantly reduced hypertrophy (based on heart size and mass; $p < 0.05$, TuD-29-tg versus WT) and preserved heart function (Figures 4A and 4B). These findings were further supported by subsequent gravimetric measures collected postsacrifice, which showed that TuD-29-tg mice had significantly lower heart weights (normalized to tibia length, HW/TL), relative to WT littermates at ∼12 weeks post-TAC ($p < 0.01$; Figure 4C). This was also reflected in histological assessments, in which TuD-29-tg hearts showed reduced mean cardiomyocyte cross-sectional areas (CSAs; Figure 4D) with a clear distributional shift toward lower fiber size (Figure 4E) compared to WT hearts (Kolmogorov-Smirnov test $p < 2.2e{-}16$).

To assess for potential modulation of miR-29 targets related to cardiac hypertrophy and function, we performed western blot for

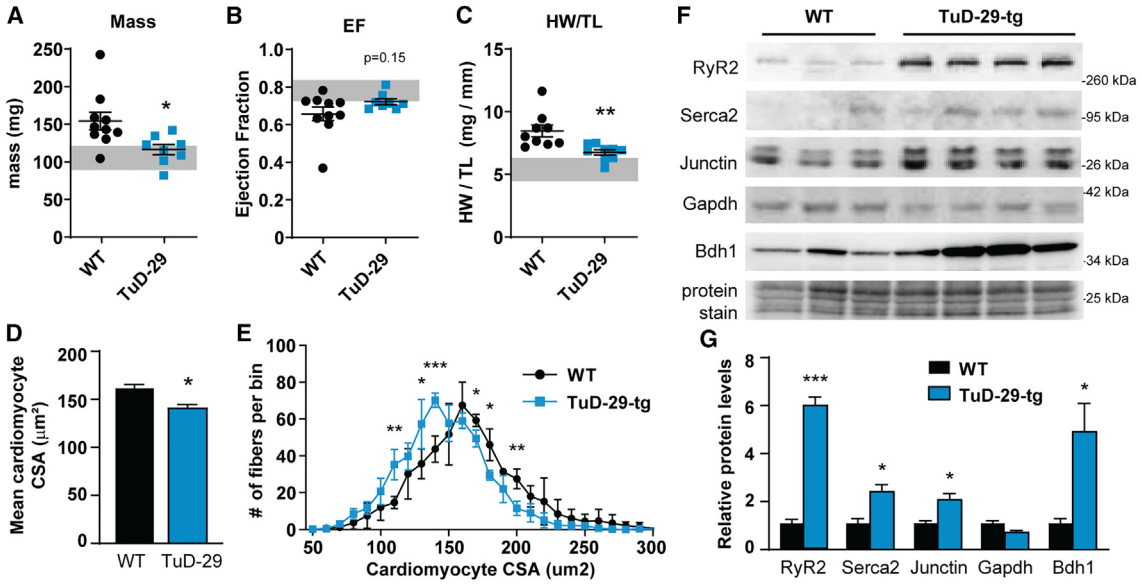

Figure 4. TuD-29 transgenic mice resist TAC-induced cardiac hypertrophy and maintain calcium handling gene expressions

Eight-week-old TuD-29-tg and WT littermate control mice (n ≥ 8/group) were subjected to surgically induced TAC to induce cardiac pressure overload and ensuing cardiac hypertrophy and dysfunction. At 10 weeks post-TAC, heart mass (A) and fractional shortening (B) were determined by echocardiography. Mice were subsequently euthanized, and HW/TL ratios were determined (C). (A–C) Normal ranges established from >30 sham-surgery control mice of similar age are indicated by the shaded box for each respective measure. (D and E) Mean cardiomyocyte CSA (D) and fiber size distributions (E) determined by histological measures are plotted (~500 fibers per mouse heart, n = 4/group). (F and G) Western blot (F) and (G) densitometry analyses were done on post-TAC tissue lysates (n ≥ 3/group) to quantify the myocardial expression levels of calcium handling proteins that are known gene targets of miR-29. All of the data are plotted as mean ± SEM. p values were determined by 2-tailed unpaired t tests. *p < 0.05; **p < 0.01; ***p < 0.001.

Serca2a, Ryr2, and Junctin, which are Ca^{2+}–related cardiomyocyte-enriched proteins (mRNAs) that we previously identified and validated as miR-29 targets.[25] Western blot data revealed a clear ~2- to 6-fold elevation in these Ca^{2+} handling proteins in TuD-29-tg mouse hearts, relative to WT hearts (Figures 4F and 4G), supporting that miR-29 is functionally inhibited in TuD-29-tg mice. Overall, these data corroborate prior findings from Sassi et al.[23] showing that miR-29 inhibition blunts the hypertrophic response in the setting of cardiac pressure overload and demonstrate the *in vivo* efficacy of our TuD-29 construct to modulate cardiac structure/function and calcium handling gene expression.

miR-29 inhibition improves cardiac filling during diastole and increases CO

To begin translating TuD-29 toward potential gene therapy applications, we assessed the effects of viral-mediated miR-29 inhibition in mice by generating and testing a cardiotropic AAV9 vector encoding the TuD-29 transgene and GFP to monitor myocardial transduction efficiency (Figure 3A). Male C57BL/6J mice (3–5 weeks old) were injected intrajugularly with either AAV:TuD-29 or control vectors (AAV:TuD-Ctrl, a scramble control TuD, or AAV:GFP) and assessed by echocardiography at 3 weeks postinjection. Mice treated with AAV:TuD-29 showed an ~20% increase in EDV and corresponding increases in SV and CO, relative to control mice treated with AAV:TuD-Ctrl and AAV:GFP (Figure 5A; Table S2). Mice were subsequently euthanized to assess the degree of AAV transduction and miR-29 inhibition. Gross immunohistological examination revealed very high AAV transduction (>90% of cardiomyocytes were GFP^+) across the treatment groups (Figure 5B). qRT-PCR revealed that miR-29a levels were reduced by ~20% in AAV-TuD-29-treated hearts, relative to controls (Figure 5C); notably, among the miR-29 family, miR-29a is the most abundantly expressed member in cardiomyocytes (>5-fold over miR-29b/c, based on publicly available data for miRNA-seq done on isolated adult mouse cardiomyocytes[27]). It is also important to note that that the degree of miR-29 inhibition mediated by TuD-29 is likely even greater than detected by miRNA quantitation, given that TuD RNAs primarily act via miRNA sequestration, not degradation. Overall, these findings suggest that miR-29 inhibition by AAV:TuD-29 treatment may acutely influence myocardial compliance and relaxation to improve diastolic function, presumably through modulating the expression of ECM and Ca^{2+} handling proteins.

Acute miR-29 overexpression in mice induces signs of diastolic dysfunction

Previous independent reports show that miR-29 levels are increased in aging tissues (including heart) in humans and rodents, and our reanalysis of available datasets indicate that miR-29 target genes are coincidentally downregulated (Figure 1). However, the biological effects of elevated miR-29 levels on cardiac structure/function and myocardial gene expression remain understudied. To address this, we treated mice with cardiotropic AAV9 that coexpresses the primary

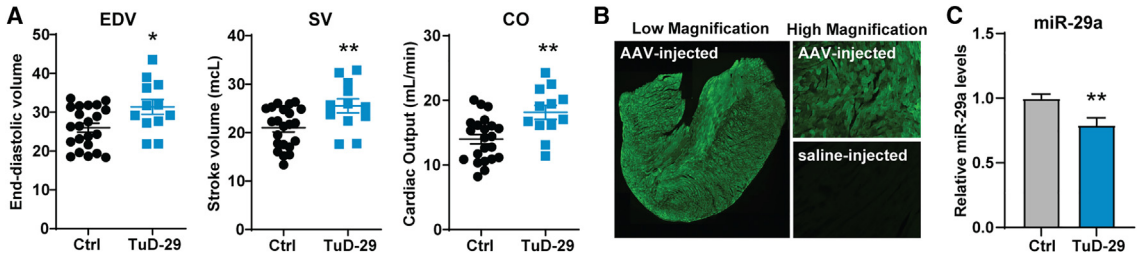

Figure 5. miR-29 inhibition improves cardiac filling during diastole and increases CO

Three-week-old male C57BL/6J mice were injected (intrajugular) with either AAV:TuD-29 (coexpresses GFP, see Figure 3A) or control (Ctrl) AAVs (AAV:TuD-Ctrl or AAV:GFP, combined into 1 group) (n ≥ 10 mice per virus). At 3 weeks postinjection, EDV, SV, and CO were determined by echocardiography (A). Mice were subsequently euthanized to assess the degree of AAV transduction by immunostaining heart tissue sections for GFP reporter expression (B, representative image shown), and miR-29 inhibition was assessed by performing qRT-PCR to measure levels of mature miR-29a in small RNA fractions isolated from the hearts (C). Plotted data are represented as the mean ± SEM; p values were obtained using 2-tailed t tests. *p < 0.05; **p < 0.01.

miR-29a transcript and GFP (Figure 6A). At 3 weeks posttreatment, echocardiography showed that AAV:miR-29a mice had an ∼25% decreased EDV and corresponding decreases in SV and CO, relative to control mice treated with AAV:GFP (Figure 6B; Table S3). Mice were subsequently euthanized to assess the magnitude of mature miRNA overexpression by qRT-PCR, which revealed an ∼8-fold increase in miR-29a levels, in AAV:miR-29a-treated versus AAV:GFP control hearts (Figure 6C). Notably, these overall findings mirror our observations with AAV-mediated miR-29 inhibition (Figure 5), providing complementary data from gain- and loss-of-function studies in mice that support a role for miR-29 in regulating diastolic function and ultimately CO.

Acute miR-29a overexpression leads to repression of a diverse set of gene targets and pathways

To gather further insight into how miR-29 may influence cardiac structure/function, we performed mRNA-seq on myocardial RNA samples collected from mice at 3 weeks postinjection with either AAV:miR-29a or AAV:GFP control. Differential expression analyses revealed many significantly altered genes between treatment groups, with an obvious broad downregulation of miR-29 targets in mice injected with AAV:miR-29a (Table S4). Cumulative distribution analyses show that miR-29 mRNA targets were significantly shifted toward reduced expression levels (Figure 6D). Furthermore, unbiased assessment of heptamer sequence frequencies across mRNAs indicated that heptamers matching miR-29 seed target sequences were the most significantly enriched heptamers among downregulated mRNAs (across both coding and 3′ UTRs[30]) in miR-29a overexpression mice (Figure 6E). Together, these findings provide strong support that the level of miR-29a overexpression achieved was capable of functionally downregulating a vast set of miR-29 target mRNAs. Gene set enrichment and pathway analyses (using ToppFun, ToppGene Suite[31]) performed on genes that were significantly downregulated in AAV:miR-29a samples ($p < 0.01$, >0.15 log2 fold change versus AAV:GFP samples) indicated that miR-29a overexpression broadly coordinated the repression of genes involved in responses to isoproterenol (a prohypertrophic β2-adrenergic receptor agonist), extracellular stimuli, nutrients, and endoplasmic reticulum (ER) stress, as well as lipid and ketone metabolism and ECM remodeling (Figure 6F and Table S5). Notably, genes that were significantly upregulated in AAV:miR-29a samples ($p < 0.01$, >0.15 log2 fold change versus AAV:GFP) were enriched for genes related to mitochondrial biogenesis and energy production, hypertrophic cardiomyopathy, contractility, and protein synthesis (translation and ribosome biogenesis), likely reflecting the prohypertrophic effects of miR-29 (Table S6).

We next examined the mRNA-seq data at the gene level and noted that the most significantly downregulated gene (based on p value, AAV:miR-29a versus AAV:GFP) was Col4a5, which encodes a flexible type IV collagen and is among the top 5 predicted miR-29 targets per the TargetScan algorithm.[11] Oddly, the reduction in Col4a5 mRNA was not reflected at the protein level by western blot (only a trend toward slight reduction was found; data not shown), perhaps due to longer protein half-life. With respect to Ca^{2+} handling genes that we previously examined, we found that Junctin (Asph) was significantly downregulated at the mRNA level in AAV:miR-29a-treated hearts versus AAV:GFP, and this was corroborated at the protein level by western blot (Figures 6G and 6H). We also selected various other targets from the mRNA-seq data to examine miR-29a-mediated target suppression more broadly at the protein level. We focused on genes with miR-29 binding sites (computationally predicted and/or sites physically bound by Ago2-RISC complexes in human cardiac tissues[11,25]) and further narrowed our selection based on mRNA expression in cardiomyocytes and potential relevance to cardiac structure/function, electrical remodeling, metabolism, and cell stress. These included Kcnip2 (KChIP2; responsible for *Ito* current) and Bdh1 (major rate-limiting enzyme in ketone metabolism), which were among the 40 most significantly downregulated genes at the mRNA level (AAV:miR-29a versus AAV:GFP), as well as p62/Sqstm1 and Ireb2, which have implicated roles in HFrEF- and HFpEF-related pathogenic pathways (autophagic, oxidative and ER stress, and iron deficiency and ferroptosis).[32–35] Notably, western blotting for these miR-29a target genes revealed clear reductions in their protein levels (generally ∼30%–40%, $p < 0.05$), with Bdh1 levels strikingly reduced by >90% ($p < 0.01$). Together, these

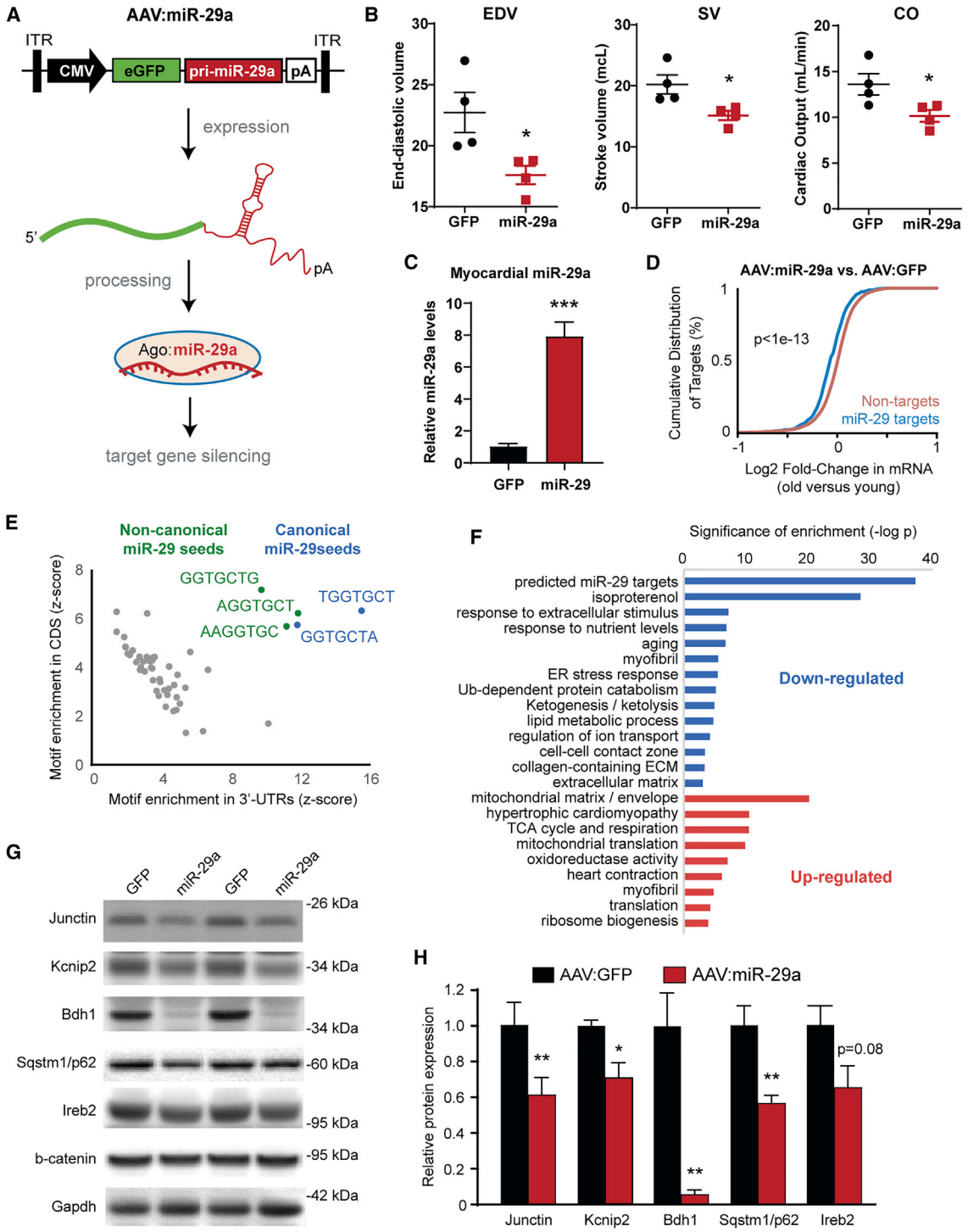

Figure 6. Acute miR-29 overexpression in mouse heart induces signs of diastolic dysfunction and downregulates a diverse array of gene targets and pathways

(A) Schematic of AAV:miR-29a vector that coexpresses primary miR-29a transcript and GFP reporter under control of the CMV promoter. (B) Three-week-old male C57BL/6J mice were injected (intrajugular) with either AAV:miR-29a or AAV:GFP control. At 3 weeks postinjection, EDV, SV, and CO were determined by echocardiography. (C) Mice were subsequently euthanized to assess the degree of and miR-29a overexpression by qRT-PCR to measure levels of mature miR-29a in small RNA fractions isolated from the hearts (C). (D–F) mRNA-seq was performed on myocardial RNA samples collected from these mice, and differential gene expression analyses were done to compare

(legend continued on next page)

data demonstrate that miR-29a is versatile in functionally repressing mRNA levels for hundreds of gene targets with diverse functions and potential relevance to HFpEF (e.g., myocardial wall stiffness, metabolic rewiring, cell stress) and provide general support that the observed mRNA decreases in AAV:miR-29a-treated hearts are also reflected at the protein level.

Given that miR-29 caused such a profound reduction in Bdh1 and that Bdh1 is upregulated in TAC hearts and its overexpression is cardioprotective,[36] we considered Bdh1 as one particular target of interest that may have contributed, in part, to blunted TAC responses in TuD-29-tg mice. Thus, we performed western blot on our previous TAC heart lysates and found that TuD-29-tg mice had ∼4-fold higher Bdh1 levels versus WT littermates (Figures 4F and 4G; $p < 0.05$). In addition to maintained Ca^{2+} handling protein expressions in TuD-29-tg mouse hearts, elevated Bdh1 may also be biologically significant, and future investigations are needed to further assess how this newfound miR-29:Bdh1 axis influences cardiac biology and disease.

DISCUSSION

This study began with our interest in understanding the biological relevance of miR-29 activity in the heart, which was inspired by observations that cardiac miR-29 expressions are high in cardiomyocytes and increased with aging.[18,19,23] Here, we provide complementary data indicating that miR-29 target gene mRNAs are broadly decreased in hearts collected from aged (versus young) humans and rodents. One noteworthy limitation is that the public data used for these analyses lack information on actual miR-29 levels in each of the samples, and thus these analyses only correlatively, not directly, link prior published observations of miR-29 elevations in aging hearts (and other tissues) to decreases in miR-29 target gene expressions, as shown in Figure 1. To further investigate the role of miR-29 in cardiac biology, we focused on miR-29 functions primarily in cardiomyocytes, which we and others found to express miR-29 family members at higher levels compared to nonmyocyte cardiac cells (e.g., endothelial and fibroblasts).[23] In NRCM studies, we demonstrate that miR-29 overexpression robustly induces cell hypertrophy, whereas miR-29 inhibition blunts hypertrophic responses after PE treatment. The latter was further complemented with data from our *in vivo* studies, in which we found that miR-29 inhibition in TuD-29-tg mice blunts TAC-induced hypertrophic responses. Together, these findings corroborate and complement previously published data by Sassi et al., who made similar observations in genetic models of reduced miR-29 expression in multiloci partial knockout mice.[23]

Moving beyond genetically engineered mice, we adapted and combined AAV9 and Tough Decoy technologies to develop viral-based miR-29 inhibition vectors to be used for biological and potentially therapeutic applications. We demonstrate the effectiveness of these vectors in repressing miR-29 expression in mouse hearts, which surprisingly led to increased diastolic filling and CO after just 3 weeks posttreatment. These findings have potential significance to clinical conditions hallmarked by diastolic dysfunction (e.g., HFpEF), typically resulting from increased myocardial wall stiffness and impaired relaxation, which may be caused by adverse ECM remodeling and improper Ca^{2+} handling, respectively, both of which are notable pathways influenced by miR-29. Although these findings are encouraging, some limitations exist. For example, in this first-generation vector, we used the constitutively active U6 promoter, which likely drives TuD-29 expression and miR-29 inhibition in other tissues targeted by AAV9; however, the biological impact of this on the observed cardiac phenotypes remains unknown. Moving forward, efforts are needed to generate and test cardiac-specific TuD-29 expression cassettes to improve specificity, because suppressing miR-29 activity in other cell types could have adverse consequences (e.g., miR-29 reduction or inhibition in fibroblast may promote tissue fibrosis[15,16] or contribute to endothelial cell dysfunction[37]).

Despite several studies supporting that miR-29 plays important roles in cardiac biology and disease, the mechanisms by which this occurs remain largely unclear due to the lack of empirical data for miR-29 functional targeting at the transcriptome-wide level in the heart. Prior studies evaluate myocardial transcriptome changes in mice with genetic reduction in miR-29[38]; however, the chronic nature of these models makes it challenging to discern direct versus indirect (i.e., downstream) effects. Here, we describe the first comprehensive mRNA-seq dataset characterizing the acute effects of miR-29 overexpression in mouse heart. These data reveal that miR-29 operates by repressing a diverse array of gene targets, the vast majority of which are conserved between mice and humans (per TargetScan). Although others have focused on the role of miR-29 in the regulation of the ECM through the regulation of collagens and Wnt signaling,[15,23,26] our data also point to broad and robust effects on hypertrophic signaling, aging, ion transport, calcium handling, unfolded protein response, ER and oxidative stress, and ketone/lipid metabolism, all of which can contribute to influencing cardiac function and shaping the course of HFpEF onset and progression.[32–35,39] Bdh1 was one of the most notably downregulated genes following miR-29 overexpression in mouse hearts, and Bdh1 overexpression has been shown to be cardioprotective

treatment groups, AAV:miR-29a versus AAV:GFP. (D) Cumulative fraction analysis of the gene expression data show that levels of miR-29 target gene mRNAs (blue) are broadly downregulated (i.e., leftward shifted), relative to nontarget genes, red) in AAV:miR-29a-treated hearts relative to AAV:GFP. Kolmogorov-Smirnov test p values are provided. (E) Plot showing the most significantly enriched heptamer sequences present in downregulated mRNAs (in both 3′ UTR and coding sequences [CDS]), based on cWords algorithm *Z* scores.[30] Sequences complementary to miR-29a are highlighted in green and blue. (F) Gene Ontology analyses performed on genes that were significantly down- or upregulated after AAV:miR-29a treatment ($p < 0.01$, >0.15 log2 fold change versus AAV:GFP samples). (G and H) Western blot analyses were performed on myocardial protein lysates harvested from mice 3 weeks postinjection with either AAV:miR-29a or AAV:GFP to assess whether select miR-29a target genes were also downregulated at the protein level. Densitometry analysis was performed to quantify expression levels, normalized to β-catenin or GAPDH loading controls. Data are represented as the mean ± SEM (n = 4/group) and p values were obtained by 2-tailed unpaired t test.

in mice subjected to TAC.[36] Bdh1 mRNA contains several conserved (in humans and mice) miR-29 binding sites in its 3′ UTR, which are engaged by Ago2 in human hearts (unpublished HITS-CLIP data from our lab). Bdh1 plays an essential role in ketone body oxidation, which is activated in failing hearts[40,41] and is being considered as a therapeutic target; thus, it is interesting to speculate that miR-29:Bdh1 interaction could serve as a potential avenue for intervention. In our studies, whether decreased Bdh1 contributed to impaired diastolic filling after miR-29 overexpression remains unclear; follow-up studies to tease this out are warranted given that ketone metabolism is thought to protect against diastolic dysfunction.[42]

Although our mRNA-seq data provide an initial useful resource to better understand miR-29 functions in cardiomyocytes, it provides only a snapshot of gene expression after 3 weeks of miR-29 overexpression. To better discern potential mechanisms related to therapeutic manipulation of miR-29, a more comprehensive mRNA-seq study is needed to further define miR-29 target gene fluctuations in mouse models of HF. Nevertheless, our current dataset can be further explored for additional miR-29 target interactions related to cardiac dysfunction and arrhythmias, and likely beyond. For example, miR-29 has been implicated in atrial fibrillation and general aging. Of note, our gene enrichment and pathway analyses identified "aging"-related genes among the top hits, as well as a strong signal for genes that change after isoproterenol treatment. The latter is interesting given the strong prohypertrophic effects of miR-29 in cardiomyocytes, and the underlying mechanisms are not completely resolved, warranting further investigations.

In summary, our studies demonstrate that viral-mediated miR-29 inhibition improves CO, whereas miR-29 overexpression impedes it. More important, this work corroborates several findings from previous studies using genetic (partial knockout) models of miR-29 reduction.[23] These results have implications for cardiac aging and heart failure, with a potential stronger relevance to HFpEF based on our gain- and loss-of-function data from mouse studies, which showed inverse effects on diastolic filling. It is clear that miR-29 plays many biological roles (in cardiomyocytes and other cell types) well beyond its established role in ECM remodeling, which has been mostly studied in fibroblasts. This is supported in particular by unpublished human heart Ago2 CLIP data recently obtained in our lab, which unveiled >100 new cardiomyocyte-enriched gene targets of miR-29, including FNDC5/Irisin, SPEG, and SCN5A/NaV1.5, which have been implicated in cardiac metabolism, oxidative stress, Ca^{2+} handling, arrhythmias, and heart failure.[43–45] It is interesting that our data here suggest that miR-29 action in cardiomyocytes also likely contributes to ECM remodeling (e.g., through regulation of flexible type IV collagens Col4a5 and Col4a2, which were downregulated after miR-29 overexpression per our mRNA-seq data) and that miR-29-mediated co-regulation of Ca^{2+} handling (and perhaps metabolic) genes in parallel may coordinately couple contraction/relaxation dynamics with myocardial compliance. Further experimentation and efforts will be needed to more firmly establish this and to develop and test cardiomyocyte-specific miR-29 inhibition vectors and assess their long-term effects on cardiac structure and function in normal mice and models of heart failure.

MATERIALS AND METHODS

Plasmids

To create the miR-29 target reporter plasmid, a synthetic DNA oligo with the sequence 5′- CTCGAGGAAGGTGCTACCTCGAAATGCT GCAACCAAGGTGCTAGGTTGCCCGCAAGGTGCTAGCGGCCG C-3′ containing three miR-29 binding sites (Integrated DNA Technologies, Coralville, IA) was introduced downstream of the Renilla luciferase expression cassette (using XhoI and NotI restriction enzyme sites) in the psiCheck2 dual luciferase plasmid (Promega, Madison, WI). The pAAV2/5:U6-TuD-Ctrl (TuD-Ctrl, scrambled Tough Decoy control) construct was previously described.[46] pAAV2/5:U6-TuD-29 (TuD-29) shuttle plasmid was constructed by inserting DNA oligo sequences (Integrated DNA Technologies) to express the following TuD stem-loop sequence from the U6 promoter: GACGGCCTCGAGACT GGCAATAATTGATTCGCGATGGTGCTACAAGTATTCTGGTC ACAGAATACCAATAATTGATTCGTGATGGTGCTACAACTAG TCTCGGGGCCGTCTT, cloned into a custom version of pFBAAV-mU6mcsCMVeGFPSV40pA (ID G0347 University of Iowa Viral Vector Core [UIOWA VVC] Facility, Iowa City, IA).

AAV2/9 vectors

AAV TuD (−29 and -Ctrl) and GFP control vectors were generated at the UIOWA VVC and contain vector genomes flanked by AAV2-type inverted terminal repeat sequences, packaged into AAV serotype 9 capsids, using the baculovirus-based method. Shuttle plasmids pAAV2/5:U6-TuD-29 and pAAV2/5:U6-TuD-Ctrl, described above, were supplied to the UIOWA VVC to generate custom AAV preparations. AAVs were purified by iodixanol gradient and subsequent ion exchange using MustangQ Acrodisc membranes (Pall, East Hills, NY). Titers of purified AAV preparations (vector genomes per milliliter [vg/mL]) were quantified by qPCR. AAV2/9-CMVeGFP-pri-miR29a aliquots were a gift from Dr. Ayotunde Dokun, who purchased the custom AAV preparation from Vigene (Rockville, MD) and had the titering done in-house at the UIOWA VVC.

Test of TuD-29 construct in N2a cells

Mouse Neuro2a (N2a) cells (CCL-131; American Type Culture Collection, Manassas, VA) were plated at 80,000 cells/well in 24-well tissue culture dishes and, 24 h later, were cotransfected with 100 ng miR-29 target reporter plasmid plus 10 nM either control miR-Neg or miR-29a pre-miRNA synthetic oligos (Ambion, Austin, TX), along with 100 ng either TuD-Ctrl plasmid or TuD-29 expression plasmids, using Lipofectamine 2000 (Thermo Fisher Scientific, Waltham, MA), completed in triplicate for each treatment combination. At 48 h posttransfection, FF and R luciferase activities were measured using a GloMax Microplate Reader and Dual Luciferase Kit reagents (Promega). Briefly, culture media was removed and 200 μL Passive Lysis Buffer was pipetted into each well, and the plate

placed on a shaker for 15 min at room temperature. Then, 10-μL lysate was transferred to duplicate wells of a 96-well white plate. Luminescence from FF and R was determined from 5-s reads after the injection of respective substrates to each well. The R/FF ratio was calculated and adjusted relative to the control (set to "1"), and results are expressed as the mean ± SEM (n = 4/group).

Rodent studies

All of the animal studies were approved by the Institutional Animal Care and Use Committees at UIOWA, and all of the experiments conform to the appropriate regulatory standards. Rodents were housed in a controlled-temperature environment on a 12-h light/dark cycle, with food and water provided *ad libitum*. Animal age and sex are noted within the paper where appropriate. For all AAV studies, C57BL/6J mice were purchased from Jackson Laboratories (stock no. 000664). TuD-29-tg mice were generated by the UIOWA Genome Editing Facility using standard methods. In brief, zygotes from 4-week-old B6SJLF1/J mice (Jackson Laboratory, stock no. 100012) were harvested, subjected to pronuclear injection with purified plasmid-derived DNA fragments encompassing a U6-driven TuD-29 expression cassette, and then implanted into pseudopregnant female mice. The resulting offspring were genotyped to identify mice carrying the transgene, and positive mice were subsequently backcrossed to the C57BL/6J strain (Jackson Laboratory, stock no. 000664) for more than three generations before experiments.

TAC

Minimally invasive TAC was performed as previously described, with few changes.[47] At the level of the suprasternal notch, a thyroid retraction and partial sternotomy was used to visualize the aortic arch on 8-week-old TUD-29 or WT male mice anesthetized with ketamine/xylazine (100/10 mg/kg, intraperitoneally). The aorta was isolated and then constricted with a titanium ligating clip (Teleflex, Wayne, PA; catalog no. 005200) gapped on 38G acupuncture needles and placed between the right innominate and left common carotid arteries. Heart structure and function was evaluated by echocardiography. Mice were euthanized and hearts were harvested and measured 10 weeks after TAC.

Echocardiography

Echocardiography was performed on conscious mice, with mild sedation (midazolam, 5 mg/kg, subcutaneously) restrained in the operator's hand, using a Vevo2100 imaging system (VisualSonics, Toronto, ON, Canada). Two-dimensional cine loops were acquired in both long- and short-axis planes to measure standard parameters of cardiac structure and function, according to the endocardial and epicardial area protocol.

Cardiomyocyte cross-sectional area measures

Cardiomyocyte area (i.e., fiber size) was determined as described.[23] Tissue sections (10 μm) were cut from mouse hearts embedded in optimal cutting temperature (OCT) compound and then fixed with 4% paraformaldehyde (PFA) in PBS for 10 min at room temperature. Tissue sections were subsequently stained with Alexa Fluor 488-conjugated wheat-germ agglutinin (Life Technologies, Carlsbad, CA; 1:200 dilution) for cell border determination. Microscopy images were taken from areas of transversely cut muscle fibers and the area of each cardiomyocyte (∼500 fibers per mouse sample) was measured manually using ImageJ (NIH).

Virus jugular vein injection

C57BL/6J mice (3–5 weeks old) were anesthetized using 1.5%–2% isoflurane inhalation. The appropriate plane of anesthesia was determined based on observations of spontaneous respiration and pain reflexes. Hair was removed from the surgical site. Preincision, 2.5 mg/kg of flunixin meglumine was subcutaneously injected. A small incision was made through the skin to expose the jugular vein. Recombinant AAV or vehicle was injected into the jugular vein using a 30G needle, delivering ∼3e−11 to 3e−12 vg/mL of AAV per mouse depending on mouse weight. The incision was subsequently sutured with 6-0 prolene suture.

Cardiomyocyte isolation

NRCMs were isolated from 1- to 3-day-old pups from Sprague-Dawley rats (Charles River, Wilmington, MA; stock no. 001) as previously described,[48] using the Worthington Neonatal Cardiomyocyte Isolation System (Worthington Biochemical, Lakewood, NJ; catalog no. LK003300) followed by a two-step Percoll density gradient, and cultured in cardiomyocyte growth media (DMEM/F12 media supplemented with 5% horse serum, 10 mM HEPES, 1% Insulin-Transferrin-Selenium (ITS), 15 μg/mL gentamycin, and 100 μM bromodeoxyuridine).

NRCM surface area measurement and live-cell calcium imaging

NRCMs were cotransfected with synthetic pre-miRNAs (10–25 nM) along with 100 ng of an EGFP expression plasmid, using Lipofectamine 2000 (Life Technologies). The transfected cells were incubated for 4 h before the transfection medium was removed and replaced with a growth medium. The cells were incubated at 37°C in a 5% CO_2 incubator for 48–72 h with daily medium exchanges before experiments. Transfected (GFP^+) NRCMs were examined with an Olympus IX70 inverted fluorescence microscope with a DP70 camera and DP Controller 2.1 software. The cell surface area was determined for 50 cardiomyocytes from at least 5 random fields. All images were analyzed by ImageJ.

For calcium imaging, NRCMs were loaded with Rhod-2 AM (AAT Bioquest, Pleasanton, CA, catalog no. 21062) at room temperature for 30 min, followed by deesterification in Tyrode's solution (containing NaCl 140 mM, NaH_2PO_4 0.33 mM, KCl 5.4 mM, HEPES 10 mM, 1.8 mM Ca^{2+}, pH 7.4, with NaOH) for 15 min. Line scan confocal images were acquired at a sampling rate of 1.93 ms per line using a 63×, 1.3 NA oil immersion objective mounted on a Zeiss LSM 510 confocal microscope (Carl Zeiss MicroImaging GmbH, Oberkochen, Germany). Steady-state Ca^{2+} transients were achieved by a 30-s pacing at 1-Hz field stimulation. All of the digital images were processed using IDL 8.0.

Luciferase-based protein synthesis assay

NRCMs were plated in growth media at 250,000 cells per well in 48-well plates. The following day, NRCMs were cotransfected using Lipofectamine 2000 (0.5% v/v, final) with psiCHECK2 (dual luciferase; FF and R) plasmid (20 ng), TuD plasmid (200 ng), and preMiRs (25 nM)) diluted in Optimem media at a final volume of 100 μL per well. The transfected cells were incubated for 4 h and then 150 μL of growth media was added per well. The next day, the media was removed and replaced with serum-free cardiomyocyte media. After at least 4 h, PE was added (100 μM, final concentration in serum-free media) and cells were incubated for ∼48 h, with media exchange after 24 h. After 48 h, media was removed and NRCMs were lysed/scraped in 100 μL per well of passive lysis buffer (Promega E1941, diluted 1:5 with water). Dual-Glo Luciferase assays were performed to measure FF and R luciferase activities (Promega E2940). Lysates (10 μL per well) were loaded into white, opaque 96-well plates in duplicate, and analyzed on a GloMAX 96-well reader with dual injectors using a dual injector protocol; where 45 μL of FF buffer and 45 μL of R buffer were sequential added with a 2-s delay and a 3-s read time per addition. Raw luciferase data for FF and R were analyzed separately and normalized to the untreated control group. PE-induced luciferase was calculated as PE treated normalized to control treated, and finally, normalized FF and R values were averaged together.

Western blotting

Tissue lysates were generated by suspending fresh-frozen tissue pieces in lysis buffer (in millimolar amounts, 150 NaCl, 10 NaF, 5 EGTA, 5 EDTA, and 50 Tris-HCl pH 7.5 with 1.0% Triton X-100, 0.5% deoxycholate, and 0.1% SDS) with freshly added 1× protease inhibitor (Roche, Indianapolis, IN), 1 mM PMSF, and 1 mM sodium orthoavanadate, and shaking in a TissueLyser (Qiagen, Germantown, MD). After 20 min on ice, lysates were clarified by centrifugation for 10 min at 10,000 × *g* at 4°C. Protein concentration was measured in clarified lysates using a BCA Protein Assay kit (Thermo Fisher) and proteins were resolved by standard SDS-PAGE (Invitrogen NuPAGE system, Invitrogen, Carlsbad, CA) before being transferred to a 0.2-μm polyvinylidene fluoride membrane (Millipore, Burlington, MA) using NuPAGE transfer buffer (Invitrogen). The membrane was blocked with 2%–5% milk in 1× Tris-buffered saline with 0.1% Tween 20 detergent (TBS-T), after which anti-Serca2 antibody (1:1,000; Thermo Fisher, catalog no. MA3-919), anti-RyR2 (1:1,000, Thermo Fisher, catalog no. MA3-916), anti-ASPH/Junctin (1:500, LifeSpan BioSciences, Lynnwood, WA; catalog no. LS-C81640), anti-Kcnip2 (1:1,000, ABclonal Technology, Woburn, MA; catalog no. A7100), anti-Bdh1 (1:2,000, ABclonal Technology, catalog no. A3763), anti-Sqstm1/p62 (1:2,000, ABclonal Technology, catalog no. A19700), anti-Ireb2 (1:2,000, ABclonal Technology, catalog no. A6382), anti-glyceraldehyde 3-phosphate dehydrogenase (GAPDH) (1:3,000, Santa Cruz Biotechnology, Dallas, TX; catalog no. sc-25778), or anti-β-catenin (1:2,000; Sigma-Aldrich, St. Louis, MO; catalog no. PLA0230), diluted in blocking buffer was added and incubated overnight at 4°C with rocking. Membranes were washed with 1× TBS-T, incubated for 1 h with horseradish peroxidase–conjugated goat anti-mouse or anti-rabbit antibody (Jackson ImmunoResearch, West Grove, PA; catalog nos. 115–035–146 and 111–035–144) diluted 1:50,000 in blocking buffer, and then washed again. Chemiluminescence detection was performed using West Femto Maximum Sensitivity Substrate (Thermo Fisher), followed by imaging on a BioRad (Hercules, CA) Versadoc (Quantity One software used for acquisition and densitometry analyses).

Quantitative real-time PCR

Total RNA was isolated from TRIzol according to the manufacturer's instructions (Thermo Fisher) and dissolved in nuclease-free water and quantified on a Nanodrop Spectrophotometer. RNA was DNase-treated using a DNA-free kit (Thermo Fisher). RT and qPCR reactions for miRNA were performed according to the TaqMan Small RNA Assays protocol using TaqMan MicroRNA Assays for 2-step qRT-PCR (hsa-miR-29a, ID no. 002112; snoRNA135, ID no. 001230, Applied Biosystems, Thermo Fisher). Briefly, 20-μL RT reactions were set up containing 10× MultiScribe RT buffer, 2 mM deoxynucleotide triphosphate (0.5 mM each), 50 U Multiscribe Reverse Transcriptase, 6 U RNase inhibitor, 30 ng total RNA, and 1× concentrations of each TaqMan assay RT primer in the pool, on ice. The pools for RT primers were miR-29a + snoRNA135. The thermocycler conditions for RT were 16°C for 30 min, 42°C for 30 min, 85°C for 5 min, and 4°C hold. After RT, cDNA samples were diluted 3-fold by the addition of nuclease-free water. For qPCR, 10-μL reactions were set up in TaqMan Universal Master Mix II with 4 μL of diluted cDNA and a 1× concentration of the appropriate TaqMan miRNA primer/probe set, in a 384-well plate in triplicate. qPCR reactions were performed on a ViiA 7 real-time PCR system with QuantStudio software (Thermo Fisher Scientific). Relative quantification (ΔΔCt) was used to analyze results, using SnoRNA135 as the reference gene (endogenous control).

Immunohistology and fluorescence microscopy

Mouse hearts were fixed with 4% PFA in PBS, embedded in OCT, and frozen in a dry ice/ethanol bath. Cryostat sections (16 μm thick) were affixed to glass slides and permeabilized with 0.2% (v/v) Triton X-100. Slides were blocked, washed, and incubated overnight at room temperature in a humidified chamber with anti-GFP antibody diluted in blocking buffer (1:1,000, Thermo Fisher, catalog no. A-6455). After washing, sections were incubated for 4 h at room temperature with Alexa Fluor 488 conjugated secondary antibody (1:500, Thermo Fisher, catalog no. A32731). After washing, slides were mounted with a coverslip and imaged using an Olympus IX70 inverted fluorescence microscope with a DP70 camera and DP Controller 2.1 software.

mRNA-seq

Total RNA samples were isolated as described above from cardiac tissue samples collected from mice treated with either AAV:miR-29a or AAV:GFP. RNA quality assessment and sequencing were performed by the Iowa Institute of Human Genetics, Genomics Division, at UIOWA. RNA quality and concentrations were determined with the

Agilent 2100 Bioanalyzer and DropSense or Little Lunatic (Unchained Labs, Pleasanton, CA) reads. The RNA integrity number values for samples were >7.5. Illumina TruSeq Stranded mRNA Library Prep kits (Illumina, San Diego, CA) were used to prepare sequencing libraries from mRNA, followed by RT to cDNA, fragment purification, and ligation to indexed (barcoded) adaptors. Indexed libraries were pooled for multiplex sequencing and run on an SP flow cell on the Illumina NovaSeq 6000 sequencer for 100 cycles with 50-bp end reads. RNA-seq data were analyzed according to the Kallisto/Sleuth pipeline.[49,50] Reads were aligned using Kallisto version 0.43.1, to Ensemble transcriptome release 98 (119,215 transcript targets). The transcriptome was acquired on March 30, 2020 from ftp://ftp.ensembl.org/pub/release-98/fasta/mus_musculus/cdna/Mus_musculus.GRCm38.cdna.all.fa.gz. Kallisto index and Kallisto quant were run using default settings, with specific input parameters of 100 bootstraps and 16 threads. Differential gene expression was quantified using Sleuth version 0.30.0, aggregating abundance on Ensemble genes, with a two-step likelihood ratio test and Wald test. Other packages include base R version 3.6.1, biomaRt version 2.42.1, dplyr version 0.8.5, and ggplot2 version 3.2.1.

Gene Ontology analyses were performed by inputting the indicated gene sets into the using ToppFun web server tool ToppGene Suite[31] and using default settings. Results were exported, and up to the top 50 enriched terms in each "category" were tabulated in Tables S5 and S6.

Statistical analyses

Statistical analyses were performed using available software and tools (e.g., Prism GraphPad and R package), with guidance from the University of Iowa Department of Biostatistics.

DATA AND CODE AVAILABILITY

Raw and processed RNA-seq data were deposited in the NCBI GEO data repository (GSE241423) for public access. All of the other data will be made available upon written request to the corresponding author.

SUPPLEMENTAL INFORMATION

Supplemental information can be found online at https://doi.org/10.1016/j.omtn.2023.102081.

ACKNOWLEDGMENTS

This work was supported by funding from the Roy J. Carver Trust (University of Iowa to R.L.B.), the University of Iowa Distinguished Scholars Program (to R.L.B.), the NIH (HL148796 and HL144717 to R.L.B.; HL130346, HL157781, and HL157741 to L.-S.S.; the Aboud Cardiovascular Research Center T32 HL007121 [to J.M.M. and B.D.P.], and the Program of Hematology T32 HL007344 to B.D.P.), and the American Heart Association (14SDG18590008 to R.L.B. and 19POST34380640 and 23CDA1055147 to J.M.M.). We also acknowledge the University of Iowa core facilities that made significant contributions to this work, including the Viral Vector Core, Gene Editing Facility, Genomics Division, Mouse Cardiovascular Phenotyping Core, and Central Microscopy Core.

AUTHOR CONTRIBUTIONS

R.L.B. conceived and designed the project, supervised the research, and analyzed and interpreted the data. X.Z. designed and executed the experiments, curated and analyzed the data, and participated in the data interpretation. J.M.M., B.D.P., L.-S.S., and B.C. assisted with the experimental design and execution, as well as the data collection and analysis. R.L.B., X.Z., J.M.M., B.D.P., and B.C. wrote the manuscript.

DECLARATION OF INTERESTS

The authors declare no competing interests.

REFERENCES

1. Writing Group Members, Mozaffarian, D., Benjamin, E.J., Go, A.S., Arnett, D.K., Blaha, M.J., Cushman, M., Das, S.R., de Ferranti, S., Després, J.P., et al. (2016). Executive Summary: Heart Disease and Stroke Statistics-2016 Update: A Report From the American Heart Association. Circulation *133*, 447–454.
2. Tsao, C.W., Lyass, A., Enserro, D., Larson, M.G., Ho, J.E., Kizer, J.R., Gottdiener, J.S., Psaty, B.M., and Vasan, R.S. (2018). Temporal Trends in the Incidence of and Mortality Associated With Heart Failure With Preserved and Reduced Ejection Fraction. JACC. Heart Fail. *6*, 678–685.
3. He, X., Du, T., Long, T., Liao, X., Dong, Y., and Huang, Z.P. (2022). Signaling cascades in the failing heart and emerging therapeutic strategies. Signal Transduct. Target. Ther. *7*, 134.
4. Mishra, S., and Kass, D.A. (2021). Cellular and molecular pathobiology of heart failure with preserved ejection fraction. Nat. Rev. Cardiol. *18*, 400–423.
5. Ramirez Flores, R.O., Lanzer, J.D., Holland, C.H., Leuschner, F., Most, P., Schultz, J.H., Levinson, R.T., and Saez-Rodriguez, J. (2021). Consensus Transcriptional Landscape of Human End-Stage Heart Failure. J. Am. Heart Assoc. *10*, e019667.
6. Koentges, C., Pepin, M.E., Müsse, C., Pfeil, K., Alvarez, S.V.V., Hoppe, N., Hoffmann, M.M., Odening, K.E., Sossalla, S., Zirlik, A., et al. (2018). Gene expression analysis to identify mechanisms underlying heart failure susceptibility in mice and humans. Basic Res. Cardiol. *113*, 8.
7. Yang, K.C., Yamada, K.A., Patel, A.Y., Topkara, V.K., George, I., Cheema, F.H., Ewald, G.A., Mann, D.L., and Nerbonne, J.M. (2014). Deep RNA sequencing reveals dynamic regulation of myocardial noncoding RNAs in failing human heart and remodeling with mechanical circulatory support. Circulation *129*, 1009–1021.
8. Leptidis, S., El Azzouzi, H., Lok, S.I., de Weger, R., Olieslagers, S., Kisters, N., Silva, G.J., Heymans, S., Cuppen, E., Berezikov, E., et al. (2013). A deep sequencing approach to uncover the miRNOME in the human heart. PLoS One *8*, e57800.
9. Melman, Y.F., Shah, R., and Das, S. (2014). MicroRNAs in heart failure: is the picture becoming less miRky? Circ. Heart Fail. *7*, 203–214.
10. Small, E.M., Frost, R.J.A., and Olson, E.N. (2010). MicroRNAs Add a New Dimension to Cardiovascular Disease. Circulation *121*, 1022–1032.
11. Grimson, A., Farh, K.K.H., Johnston, W.K., Garrett-Engele, P., Lim, L.P., and Bartel, D.P. (2007). MicroRNA targeting specificity in mammals: determinants beyond seed pairing. Mol. Cell *27*, 91–105.
12. Kertesz, M., Iovino, N., Unnerstall, U., Gaul, U., and Segal, E. (2007). The role of site accessibility in microRNA target recognition. Nat. Genet. *39*, 1278–1284.
13. van Rooij, E., and Kauppinen, S. (2014). Development of microRNA therapeutics is coming of age. EMBO Mol. Med. *6*, 851–864.
14. Rupaimoole, R., and Slack, F.J. (2017). MicroRNA therapeutics: towards a new era for the management of cancer and other diseases. Nat. Rev. Drug Discov. *16*, 203–222.
15. van Rooij, E., Sutherland, L.B., Thatcher, J.E., DiMaio, J.M., Naseem, R.H., Marshall, W.S., Hill, J.A., and Olson, E.N. (2008). Dysregulation of microRNAs after

myocardial infarction reveals a role of miR-29 in cardiac fibrosis. Proc. Natl. Acad. Sci. USA *105*, 13027–13032.

16. Dawson, K., Wakili, R., Ordög, B., Clauss, S., Chen, Y., Iwasaki, Y., Voigt, N., Qi, X.Y., Sinner, M.F., Dobrev, D., et al. (2013). MicroRNA29: a mechanistic contributor and potential biomarker in atrial fibrillation. Circulation *127*, 1466–1475. 1475.e1-28.

17. Roncarati, R., Viviani Anselmi, C., Losi, M.A., Papa, L., Cavarretta, E., Da Costa Martins, P., Contaldi, C., Saccani Jotti, G., Franzone, A., Galastri, L., et al. (2014). Circulating miR-29a, among other up-regulated microRNAs, is the only biomarker for both hypertrophy and fibrosis in patients with hypertrophic cardiomyopathy. J. Am. Coll. Cardiol. *63*, 920–927.

18. Heid, J., Cencioni, C., Ripa, R., Baumgart, M., Atlante, S., Milano, G., Scopece, A., Kuenne, C., Guenther, S., Azzimato, V., et al. (2017). Age-dependent increase of oxidative stress regulates microRNA-29 family preserving cardiac health. Sci. Rep. *7*, 16839.

19. Rusu-Nastase, E.G., Lupan, A.M., Marinescu, C.I., Neculachi, C.A., Preda, M.B., and Burlacu, A. (2021). MiR-29a Increase in Aging May Function as a Compensatory Mechanism Against Cardiac Fibrosis Through SERPINH1 Downregulation. Front. Cardiovasc. Med. *8*, 810241.

20. Dalgaard, L.T., Sørensen, A.E., Hardikar, A.A., and Joglekar, M.V. (2022). The microRNA-29 family: role in metabolism and metabolic disease. Am. J. Physiol. Cell Physiol. *323*, C367–C377.

21. Wang, H., Wang, B., Zhang, A., Hassounah, F., Seow, Y., Wood, M., Ma, F., Klein, J.D., Price, S.R., and Wang, X.H. (2019). Exosome-Mediated miR-29 Transfer Reduces Muscle Atrophy and Kidney Fibrosis in Mice. Mol. Ther. *27*, 571–583.

22. Xiao, J., Meng, X.M., Huang, X.R., Chung, A.C., Feng, Y.L., Hui, D.S., Yu, C.M., Sung, J.J., and Lan, H.Y. (2012). miR-29 inhibits bleomycin-induced pulmonary fibrosis in mice. Mol. Ther. *20*, 1251–1260.

23. Sassi, Y., Avramopoulos, P., Ramanujam, D., Grüter, L., Werfel, S., Giosele, S., Brunner, A.D., Esfandyari, D., Papadopoulou, A.S., De Strooper, B., et al. (2017). Cardiac myocyte miR-29 promotes pathological remodeling of the heart by activating Wnt signaling. Nat. Commun. *8*, 1614.

24. Haraguchi, T., Ozaki, Y., and Iba, H. (2009). Vectors expressing efficient RNA decoys achieve the long-term suppression of specific microRNA activity in mammalian cells. Nucleic Acids Res. *37*, e43.

25. Spengler, R.M., Zhang, X., Cheng, C., McLendon, J.M., Skeie, J.M., Johnson, F.L., Davidson, B.L., and Boudreau, R.L. (2016). Elucidation of transcriptome-wide microRNA binding sites in human cardiac tissues by Ago2 HITS-CLIP. Nucleic Acids Res. *44*, 7120–7131.

26. Abonnenc, M., Nabeebaccus, A.A., Mayr, U., Barallobre-Barreiro, J., Dong, X., Cuello, F., Sur, S., Drozdov, I., Langley, S.R., Lu, R., et al. (2013). Extracellular matrix secretion by cardiac fibroblasts: role of microRNA-29b and microRNA-30c. Circ. Res. *113*, 1138–1147.

27. Matkovich, S.J., Edwards, J.R., Grossenheider, T.C., de Guzman Strong, C., and Dorn, G.W., 2nd (2014). Epigenetic coordination of embryonic heart transcription by dynamically regulated long noncoding RNAs. Proc. Natl. Acad. Sci. USA *111*, 12264–12269.

28. Nickel, A.G., von Hardenberg, A., Hohl, M., Löffler, J.R., Kohlhaas, M., Becker, J., Reil, J.C., Kazakov, A., Bonnekoh, J., Stadelmaier, M., et al. (2015). Reversal of Mitochondrial Transhydrogenase Causes Oxidative Stress in Heart Failure. Cell Metab. *22*, 472–484.

29. Zi, M., Stafford, N., Prehar, S., Baudoin, F., Oceandy, D., Wang, X., Bui, T., Shaheen, M., Neyses, L., and Cartwright, E.J. (2019). Cardiac hypertrophy or failure? - A systematic evaluation of the transverse aortic constriction model in C57BL/6NTac and C57BL/6J substrains. Curr. Res. Physiol. *1*, 1–10.

30. Rasmussen, S.H., Jacobsen, A., and Krogh, A. (2013). cWords - systematic microRNA regulatory motif discovery from mRNA expression data. Silence *4*, 2.

31. Chen, J., Bardes, E.E., Aronow, B.J., and Jegga, A.G. (2009). ToppGene Suite for gene list enrichment analysis and candidate gene prioritization. Nucleic Acids Res. *37*, W305–W311.

32. Yuan, X., Xiao, Y.C., Zhang, G.P., Hou, N., Wu, X.Q., Chen, W.L., Luo, J.D., and Zhang, G.S. (2016). Chloroquine improves left ventricle diastolic function in streptozotocin-induced diabetic mice. Drug Des. Devel. Ther. *10*, 2729–2737.

33. Costain, G., Ghosh, M.C., Maio, N., Carnevale, A., Si, Y.C., Rouault, T.A., and Yoon, G. (2019). Absence of iron-responsive element-binding protein 2 causes a novel neurodegenerative syndrome. Brain *142*, 1195–1202.

34. Beale, A.L., Warren, J.L., Roberts, N., Meyer, P., Townsend, N.P., and Kaye, D. (2019). Iron deficiency in heart failure with preserved ejection fraction: a systematic review and meta-analysis. Open Heart *6*, e001012.

35. Kitakata, H., Endo, J., Hashimoto, S., Mizuno, E., Moriyama, H., Shirakawa, K., Goto, S., Katsumata, Y., Fukuda, K., and Sano, M. (2021). Imeglimin prevents heart failure with preserved ejection fraction by recovering the impaired unfolded protein response in mice subjected to cardiometabolic stress. Biochem. Biophys. Res. Commun. *572*, 185–190.

36. Uchihashi, M., Hoshino, A., Okawa, Y., Ariyoshi, M., Kaimoto, S., Tateishi, S., Ono, K., Yamanaka, R., Hato, D., Fushimura, Y., et al. (2017). Cardiac-specific bdh1 overexpression ameliorates oxidative stress and cardiac remodeling in pressure overload-induced heart failure. Circ Heart Fail *10*.

37. Widlansky, M.E., Jensen, D.M., Wang, J., Liu, Y., Geurts, A.M., Kriegel, A.J., Liu, P., Ying, R., Zhang, G., Casati, M., et al. (2018). miR-29 contributes to normal endothelial function and can restore it in cardiometabolic disorders. EMBO Mol. Med. *10*, e8046.

38. Caravia, X.M., Fanjul, V., Oliver, E., Roiz-Valle, D., Morán-Álvarez, A., Desdín-Micó, G., Mittelbrunn, M., Cabo, R., Vega, J.A., Rodríguez, F., et al. (2018). The microRNA-29/PGC1alpha regulatory axis is critical for metabolic control of cardiac function. PLoS Biol. *16*, e2006247.

39. Selvaraj, S., Kelly, D.P., and Margulies, K.B. (2020). Implications of Altered Ketone Metabolism and Therapeutic Ketosis in Heart Failure. Circulation *141*, 1800–1812.

40. Bedi, K.C., Jr., Snyder, N.W., Brandimarto, J., Aziz, M., Mesaros, C., Worth, A.J., Wang, L.L., Javaheri, A., Blair, I.A., Margulies, K.B., and Rame, J.E. (2016). Evidence for Intramyocardial Disruption of Lipid Metabolism and Increased Myocardial Ketone Utilization in Advanced Human Heart Failure. Circulation *133*, 706–716.

41. Aubert, G., Martin, O.J., Horton, J.L., Lai, L., Vega, R.B., Leone, T.C., Koves, T., Gardell, S.J., Krüger, M., Hoppel, C.L., et al. (2016). The Failing Heart Relies on Ketone Bodies as a Fuel. Circulation *133*, 698–705.

42. Matsuura, T.R., Puchalska, P., Crawford, P.A., and Kelly, D.P. (2023). Ketones and the Heart: Metabolic Principles and Therapeutic Implications. Circ. Res. *132*, 882–898.

43. Lin, C., Guo, Y., Xia, Y., Li, C., Xu, X., Qi, T., Zhang, F., Fan, M., Hu, G., Zhao, H., et al. (2021). FNDC5/Irisin attenuates diabetic cardiomyopathy in a type 2 diabetes mouse model by activation of integrin alphaV/beta5-AKT signaling and reduction of oxidative/nitrosative stress. J. Mol. Cell. Cardiol. *160*, 27–41.

44. Campbell, H., Aguilar-Sanchez, Y., Quick, A.P., Dobrev, D., and Wehrens, X.H.T. (2021). SPEG: a key regulator of cardiac calcium homeostasis. Cardiovasc. Res. *117*, 2175–2185.

45. Zhang, X., Yoon, J.Y., Morley, M., McLendon, J.M., Mapuskar, K.A., Gutmann, R., Mehdi, H., Bloom, H.L., Dudley, S.C., Ellinor, P.T., et al. (2018). A common variant alters SCN5A-miR-24 interaction and associates with heart failure mortality. J. Clin. Invest. *128*, 1154–1163.

46. Stein, C.S., McLendon, J.M., Witmer, N.H., and Boudreau, R.L. (2022). Modulation of miR-181 influences dopaminergic neuronal degeneration in a mouse model of Parkinson's disease. Mol. Ther. Nucleic Acids *28*, 1–15.

47. Hu, P., Zhang, D., Swenson, L., Chakrabarti, G., Abel, E.D., and Litwin, S.E. (2003). Minimally invasive aortic banding in mice: effects of altered cardiomyocyte insulin signaling during pressure overload. Am. J. Physiol. Heart Circ. Physiol. *285*, H1261–H1269.

48. McLendon, J.M., Zhang, X., Matasic, D.S., Kumar, M., Koval, O.M., Grumbach, I.M., Sadayappan, S., London, B., and Boudreau, R.L. (2022). Knockout of Sorbin And SH3 Domain Containing 2 (Sorbs2) in Cardiomyocytes Leads to Dilated Cardiomyopathy in Mice. J. Am. Heart Assoc. *11*, e025687.

49. Bray, N.L., Pimentel, H., Melsted, P., and Pachter, L. (2016). Near-optimal probabilistic RNA-seq quantification. Nat. Biotechnol. *34*, 525–527.

50. Pimentel, H., Bray, N.L., Puente, S., Melsted, P., and Pachter, L. (2017). Differential analysis of RNA-seq incorporating quantification uncertainty. Nat. Methods *14*, 687–690.